

Design of self-adaptive oscillating neurons using electrically reconfigurable skyrmion lattices

Priyamvada Jadaun*, Can Cui and Jean Anne C. Incorvia
Dept. of Electrical and Computer Engineering, The University of Texas at Austin

(Dated: October 29, 2020)

*priyamvada@utexas.edu

ABSTRACT

Taking inspiration from the brain, neuromorphic computing promises to actualize the transformative potential of Artificial Intelligence (AI) by providing a path for ultra-low power AI implementation. Moreover, mimicking the complex and advanced properties of the brain can deliver a more powerful form of computation than is currently available. Here, we design and simulate a novel artificial neuron that incorporates two advanced neural behaviors: oscillatory dynamics and neuromodulation. Neuromodulation is the self-adaptive ability of a neuron to regulate its dynamics in response to its environment and contextual cues. The artificial neuron is implemented with a lattice of five magnetic skyrmions in a bilayer of insulating thulium iron garnet (TmIG) and platinum (Pt). The oscillatory dynamics of the coupled skyrmions has a multi-frequent spectrum which provides the neuron with a rich basis for information representation. Neuromodulation is enabled by the reconfigurability of the skyrmion lattice: individual skyrmions can be manipulated by electrical currents to change their arrangement in the lattice, which shifts the resonant frequencies and modulates the amplitudes of oscillatory outputs of the neuron in response to the same external excitation. Bio-mimicking dynamics such as bursting are shown. The results can be used to implement advanced neuromorphic applications including burst-coding, motion detection, cognition, brain-machine interfaces and attention-based learning.

I. INTRODUCTION

Recent years have witnessed an explosive growth in artificial intelligence (AI) that promises to transform virtually every sector of society, including healthcare, Internet of Things, education, agriculture, etc. [1, 2]. However, AI circuits that typically process large amounts of data use significant energy and area when implemented with conventional chips (CMOS) and architecture (von Neumann). A promising alternative is brain-inspired neuromorphic computing, which is a massively parallel architecture that connects myriad low-power computing elements (neurons) with adaptive memory elements (synapses), and results in an ultra-low-power implementation of AI [3]. In addition to energy efficiency, advanced neuromorphic circuits that mimic the complex behaviors of the brain can provide more powerful computational abilities than are currently available. While a simple form of neuromorphic computing uses neurons that spike in response to an input that crosses a threshold, biological neurons demonstrate more rich, adaptive and computationally powerful behavior [4, 5]. Two neuronal functions to incorporate in neuromorphic circuits are oscillatory dynamics and neuromodulation.

Although oscillatory dynamics is a critical property of the brain, its implementation in neuromorphic circuits has been very limited [6, 7]. In the brain, signal oscillations are ubiquitous at all levels of neuronal organization ranging from sub-threshold oscillations of the membrane potential in a single neuron to the macroscopic oscillations of ionic current output by an ensemble of neurons manifested in Electroencephalogram (EEG) signals. These oscillations are thought to play a critical role in a variety of mental processes such as information transfer, perception, attention, decision-making, memory [8] and feature binding [9, 10]. Incorporating oscillatory dynamics in neuromorphic circuits can unleash these cognitive functionalities and find applications in areas such as accelerated AI, artificial prosthesis, biomedicine and brain-machine interfaces.

Neuromodulation is a mechanism by which the brain controls and alters the functioning of its neural circuits in real-time, providing the brain with its ability to adapt [11]. It can alter the amplitude and frequency of oscillations in neural circuits and produce rhythmic bursts of action potentials (bursting) [4, 11]. By increasing the dynamical range of neural circuits, neuromodulation enhances the coding capacity of the brain [8]. Moreover, neuromodulation is thought to play a vital role in higher-level cognition including cue detection [12], visual perception [13], attention [9, 14] and alterations in awareness and consciousness [8].

Despite its importance, neuromodulation has not yet been incorporated into oscillatory neurons. Moreover, state-of-the-art spintronic oscillating neurons have demonstrated simple oscillatory dynamics with one resonant frequency [6, 15, 16], but little work has explored spintronic solutions with multi-frequency spectra. Spintronic nanodevices are particularly attractive for the development of neuromorphic hardware, owing to their small footprint, high endurance and low power consumption. Topologically stable chiral magnetic states (skyrmions) have been designed as spiking neurons [17, 18, 19] with the advantage of small size and the ability to be created, manipulated, detected and erased by current or field. These skyrmion-based artificial neurons display the simpler spiking properties of biological neurons but have not yet been utilized for more advanced neuronal properties such as oscillation and bursting.

Here, we design a self-adaptive, artificial neuron that incorporates both oscillatory dynamics and neuromodulation. The Tunable-SKyrmion-based Oscillating NEuron (T-SKONE) is designed using skyrmions and magnetic oscillations (spin waves), and it is validated using micromagnetic modeling. T-SKONE consists of an artificial skyrmion lattice with five skyrmion nanotracks hosted in a bilayer of insulating thulium iron garnet (TmIG) and platinum (Pt). When excited by an oscillating magnetic field, the neuron produces spin waves originating from oscillations of the skyrmion cores. Multi-frequency oscillatory dynamics are achieved due to the stray field coupling of the five side-by-side skyrmions that produces multiple resonant frequencies of the coupled system. Since each resonant frequency can represent one bit of information, the multi-frequency spectrum provides a large basis of information representation, which could be used for functions such as pattern classification of larger and more complex datasets [15]. Neuromodulation is achieved by reconfiguring the individual skyrmions' positions using applied current, resulting in a change in the resonant frequencies and amplitudes. Contextual information, encoded by modulatory currents, can therefore alter the functioning of the neuron and modulate the interpretation of the driving input information (encoded by oscillating magnetic field) being processed. This ability to modulate information imparts to T-SKONE a self-adaptive, context-

dependent response to stimuli, mimicking the dynamic intelligence of the brain and is an improvement over state-of-the-art oscillating neurons whose dynamics is not adaptive to contextual information.

Section II describes the neuron design and function in more detail. Section III examines the dynamics of T-SKONE and demonstrates that it has a strongly coupled spectrum with four resonant modes, each mode comprised of multiple resonant frequencies. We show both frequency and amplitude of the neuron oscillation are modified upon reconfiguration, implementing neuromodulation. Section IV shows that neuromodulation can be utilized to implement bursting dynamics in the neuron.

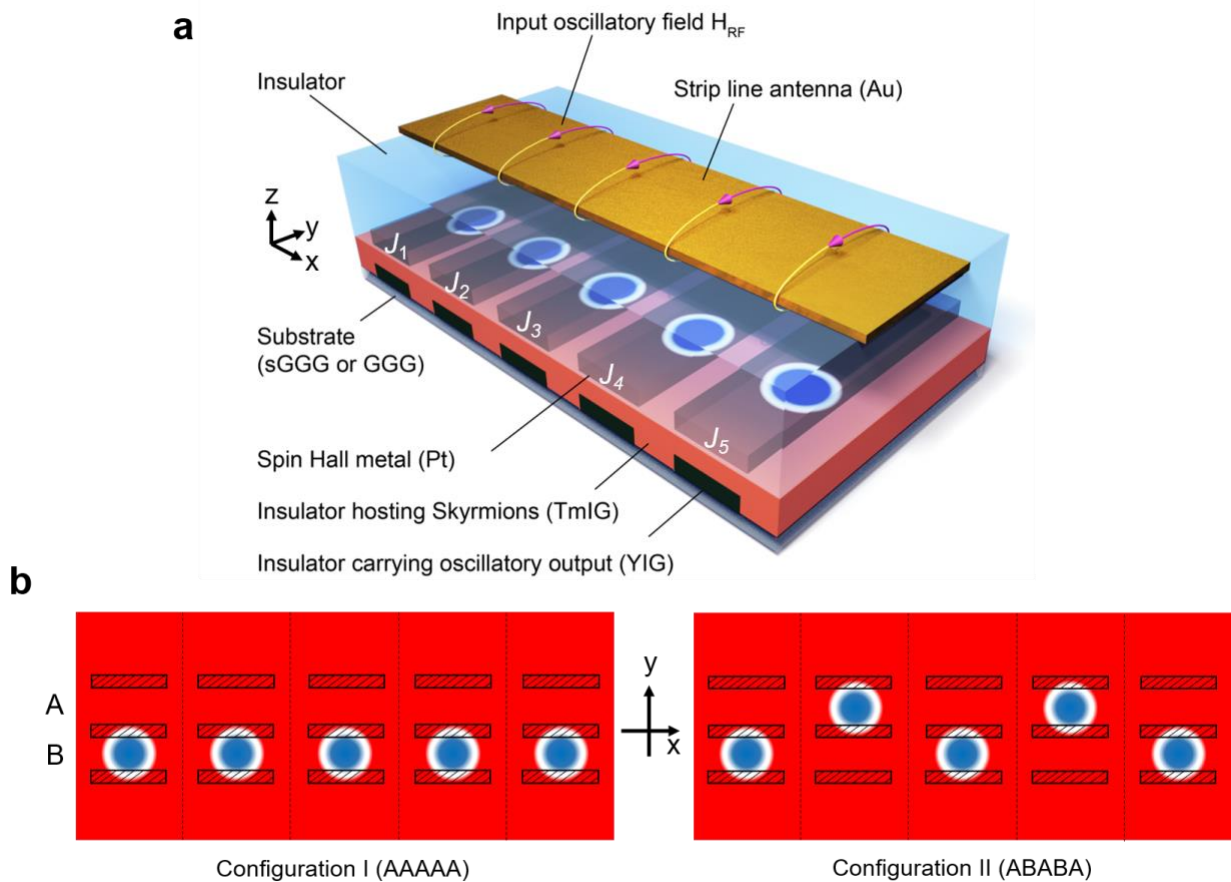


FIG. 1. Schematic of the self-adaptive oscillating neuron. (a) Structure of the neuron. TmIG (salmon): insulating magnet hosting the skyrmion lattice. H_{RF} : excitatory magnetic field input carried by strip line antenna. J_1 - J_5 : modulatory current inputs carried by the spin Hall metal (Pt). YIG: spin waves output readout. (b) Top-down views of the skyrmion lattice, with skyrmions arranged in Configuration I (AAAAA, left) and II (ABABA, right), respectively. The shadowed regions have reduced-perpendicular magnetic anisotropy, designed to softly pin the skyrmions.

II. NEURON DESIGN & FUNCTIONALITY

A schematic of T-SKONE is shown in Fig. 1 (a). The skyrmion lattice (salmon) comprises five nanotracks (with a nanotrack along y) each hosting a single skyrmion (blue), labeled Sk1-Sk5, respectively. To precisely arrange the skyrmions in the lattice and prevent skyrmion dislocation upon applying an oscillatory magnetic field, reduced-perpendicular magnetic anisotropy (PMA) regions are introduced as skyrmion pinning sites (shadowed regions in Fig.1 (b)). Such reduced-PMA regions can be created using ion implantation [20]. Since the skyrmion boundary with in-plane magnetization tends to be located in the low-PMA regions to reduce the overall magnetostatic energy [21], the skyrmions can be softly pinned into lattice sites A or B (Fig. 1 (b)). The neuron receives two types of inputs: (i) a global, excitatory magnetic field input (H_{RF}) applied to all skyrmions through the gold strip line antenna, which induces localized skyrmion oscillations and produces spin waves, and (ii) local, modulatory current inputs (J_1 - J_5) applied to individual skyrmions through the spin Hall metals Pt (purple), which independently move the skyrmions along the nanotracks in y and position them in site A or B. As the skyrmion lattice configuration is modified (e.g. between Configurations I and II as shown in Fig. 1 (b)), so are the skyrmion coupling strengths and therefore their resonant frequencies. Thus, the response of the neuron to the excitatory input can be controlled by the modulatory currents, mimicking neuromodulation. The outputs from the skyrmion nanotracks are carried by co-planar waveguides built using an insulating magnet (YIG) to be subsequently processed and combined.

Recent work has reported the observation of above and near room-temperature skyrmions in a bilayer heterostructure composed of a magnetic insulator, thulium iron garnet (TmIG, $Tm_3Fe_5O_{12}$) in contact with a spin Hall metal (Pt) [22]. There have also been experimental observations of domain wall motion in TmIG/Pt bilayers driven by spin orbit torque [23] [24]. The TmIG/Pt system provides innate electrical isolation to the individual nanotracks, while at the same time allowing the skyrmions to couple magnetically. However, since the skyrmion phase in TmIG/Pt typically exists at and above 360 K, more work is required for the design of room-temperature insulating skyrmion materials.

III. NEURONAL DYNAMICS

Simulations were carried out using the MuMax3 solver [25] (see Methods) to examine the oscillatory dynamics of T-SKONE. Three lattice configurations were studied: Configuration I (AAAAA), II (ABABA) and III (BABAB). The neuron was first excited with an external driving magnetic field of form $\text{sinc}()$ with a cutoff frequency of 60 GHz (see Methods) and then allowed to relax. Following the methods described in [26], time evolutions of skyrmion core coordinates were calculated. The fast Fourier transform (FFT) power density spectra of the skyrmion core trajectories are shown in Fig. 2 (a-c), with peaks indicating resonant frequencies of the neuron. Configuration I, II and III are plotted in blue (a), magenta (b) and green (c), respectively. There are two resonant peaks, Mode 1 and Mode 2, observed for each configuration at around 0.80 GHz and 1.04 GHz. Figure 2 (d-f) are the zoom-ins of (a-c) and extended up to 2.0 GHz, where two more resonant peaks around 1.22 GHz (Mode 3) and 1.85 GHz (Mode 4) can be observed. It is evident that a change in configuration alters both frequency and amplitude of resonant peaks. For

instance, Sk1 in Configuration I shows a peak at 1.85 GHz, which is very small for Configuration II and absent for Configuration III.

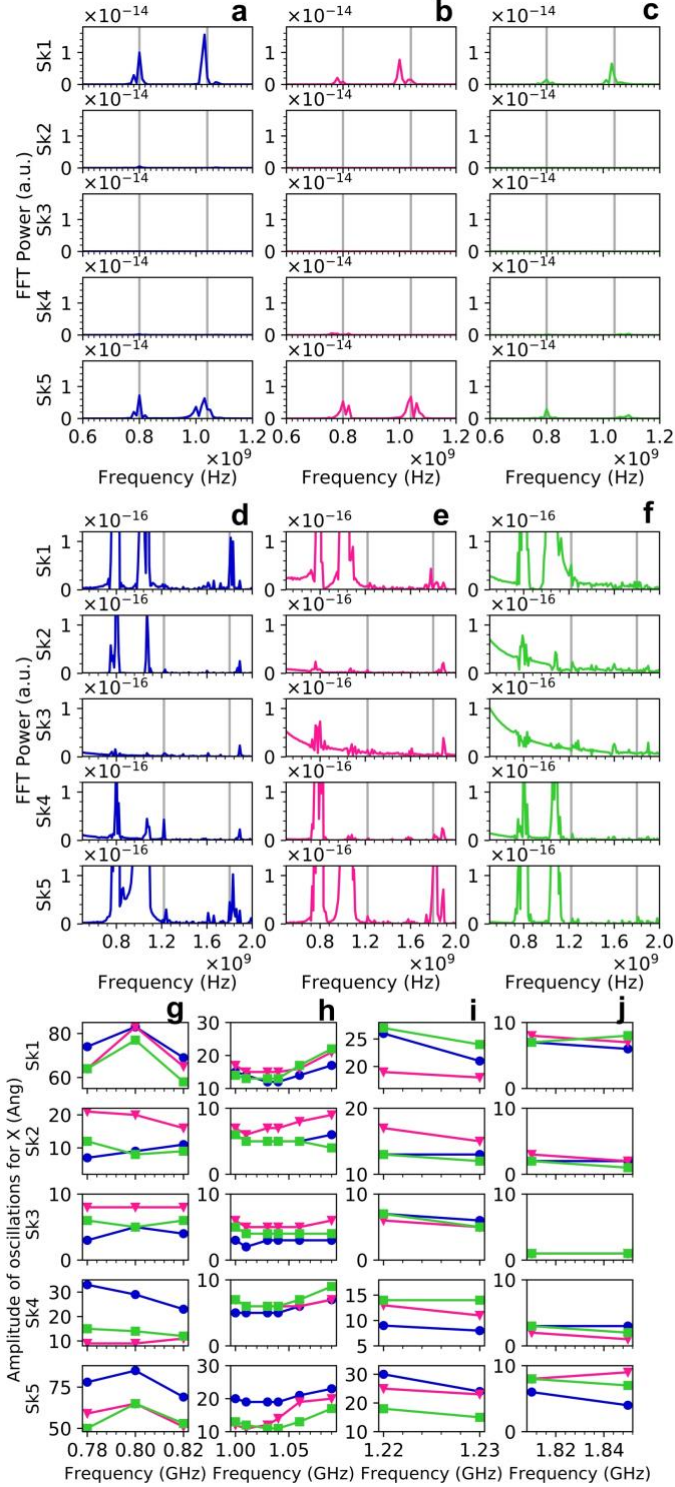


FIG. 2. Coupled dynamics of the TmIG/Pt neuron. (a-c) Fast Fourier transform (FFT) power density spectra of the neuron in Configuration I (AAAAA) (a, blue), II (ABABA) (b, magenta) and III (BABAB) (c, green), for all five skyrmions Sk1-Sk5, in response to frequency of AC magnetic field. (d-f) Zoom-in of (a-c). (g-j) Oscillation amplitudes at a range of frequencies for the three configurations.

To demonstrate neuromodulation, T-SKONE was excited with a 1 mT driving sinusoidal magnetic field at a range of frequencies, and the corresponding oscillation amplitudes were simulated. Fig. 2 (g-j) show the oscillation amplitudes along x at driving frequency ranges centered on (g) Mode 1, (h) Mode 2, (i) Mode 3, and (j) Mode 4, each for all three configurations (I blue, II magenta, and III green). Large oscillation amplitudes of up to 8 nm were observed even with a small driving field of 1 mT, promising for low energy operation of the device. For a given skyrmion driven at a certain frequency, a significant change in the oscillation amplitudes was observed as the neuron is reconfigured. Notable differences include Configuration I vs. Configurations II and III for Sk4 at Mode 1, as well as for Sk5 at Mode 1; Configuration II vs Configuration III for Sk1 at Mode 3, as well as for Sk5 at Mode 1.

Each resonant mode originates from a distinct type of skyrmion dynamics, including breathing, gyration and their hybridizations. We now discuss the four resonant modes of Configuration I. We find that Modes 1 and 3 originate from pure breathing and pure counterclockwise (CCW) gyration of the skyrmions, whereas Modes 2 and 4 are hybridization of breathing and gyrotropic modes. The neuron was excited with a magnetic field of sinusoidal form with frequency f_0 , where f_0 is one of the resonant frequencies of Configuration I. Fig. 3 (a-d) shows the skyrmion oscillations for Modes 1-4, respectively. The first two sections of Fig. 3 plot the oscillations for every skyrmion along X and Y, respectively. Periodic sinusoidal oscillations of the skyrmion core along X and Y were observed, with their frequencies locked to the driving frequency and with a wide range of amplitudes.

The physical origin of these modes is revealed by the topological charge density maps of the T-SKONE at times $t = 0, T/4, T/2$ and $3T/4$, where T is the respective time period of oscillation, as shown in the four sections on the right of Fig. 3. Fig. 3 (a) shows the skyrmion oscillation for Configuration I at Mode 1 (0.80 GHz). The oscillation amplitudes are in general larger for the outer skyrmions (Sk1 and Sk5) than amplitudes seen for inner skyrmions (Sk2-Sk4), pointing to skyrmion-skyrmion repulsion as the dominant form of interaction. The topological charge density plots demonstrate that this is a breathing mode. Notably, in this mode the neighboring skyrmions oscillate out-of-phase. This is likely because a state in which neighboring skyrmions oscillate (breathe) in synchrony and thus expand and contract together will experience strong skyrmion-skyrmion interactions.

Fig. 3 (b) plots the output for Configuration I at Mode 2 (1.04 GHz). As in Mode 1, the outer skyrmions (Sk1 and Sk5) have larger oscillation amplitudes than the inner skyrmions (Sk2-Sk4). From the topological charge density maps, a mixture of the two oscillations instead of complete cycles of breathing mode or gyration mode are observed over the time period of oscillation, which indicates that this mode is a hybridization between these two pure modes. The amplitudes for the inner skyrmions (Sk2-Sk4) are comparable, and their modes are similar in their phase ordering.

Skyrmion oscillations at Mode 3 (1.22 GHz) are shown in Fig. 3 (c) with the outer skyrmions showing much larger oscillation amplitudes than the inner skyrmions. Topological charge density plots reveal the origin of this mode to be a CCW gyration mode with all the skyrmions synchronized. Finally, Fig. 3 (d) demonstrates oscillatory dynamics at Mode 4 (1.85 GHz) where oscillations for all skyrmions are generally small (< 1 nm). Topological charge densities reveal

this to be a highly complex mode originating from the hybridization of breathing, counterclockwise and clockwise gyration.

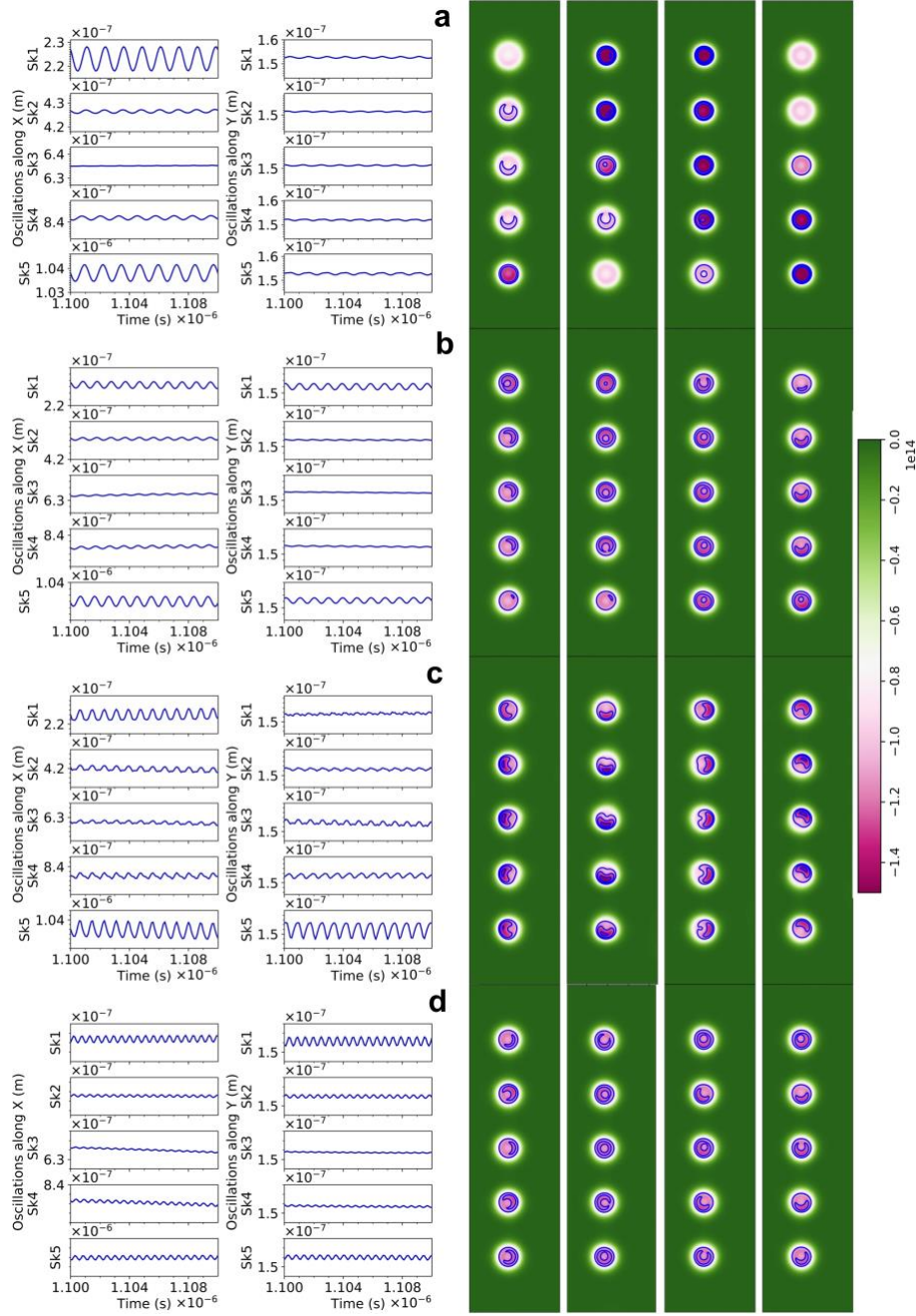


FIG. 3. Resonant modes of the TmIG/Pt based oscillating neuron in Configuration 1 when excited by a sinusoidal driving field of frequency (a) 0.80 GHz (Mode 1), (b) 1.04 GHz (Mode 2), (c) 1.22 GHz (Mode 3) and (d) 1.85 GHz (Mode 4). The two left most columns plot the output oscillations along X and Y, respectively. The four columns on the right plot the topological charge densities at times $t = 0, T/4, T/2, 3T/4$, where T is the respective time period of oscillation. The color maps for topological charge density ranges from $-1.5 \times 10^{14} \text{ m}^{-2}$ (magenta) to zero (green).

With few exceptions, the largest oscillatory amplitudes were seen for Modes 1 and 3 and the smallest were seen for Mode 4. This is likely because Modes 1 and 3 are fundamental modes whereas Modes 2 and 4 are hybridizations of the fundamental modes, with Mode 4 being a complex hybridization of three separate fundamental modes. The discovery of hybridized modes in skyrmion lattices brings to the oscillatory neuron particularly rich and coupled dynamics, enhancing its utility for neuromorphic applications. When the skyrmion lattice in Configurations I and II were excited with the same frequencies f_0 as above, they also demonstrated four modes of the same physical origin, but different oscillation amplitudes.

IV. ADDITIONAL BIO-INSPIRED DYNAMICS BASED ON NEUROMODULATION

We now demonstrate that neuromodulation of T-SKONE can lead to bursting. Continuously driven by an excitatory input with fixed frequency, the neuron was reconfigured between Configuration I and II by the modulatory input, and its real-time oscillatory output was simulated. This simulation mimics a real-world scenario where the brain processes the same information (represented by the excitatory input) in a different context (represented by the modulatory input). In Fig. 4 (a), starting at $t = 0$ ns, the neuron is in Configuration II and driven by an excitatory field of 0.80 GHz; as it is reconfigured to Configuration I at $t = 600$ ns, oscillation amplitudes of Sk2 and Sk3 significantly increase. In Fig. 4 (b), the reverse effect is demonstrated at a driving field frequency of 1.85 GHz, where Sk5 exhibits dramatic reduction of oscillation amplitude as the neuron is transitioned from Configuration II to Configuration I. The modulation of oscillatory dynamics thus implements the bursting property of neurons.

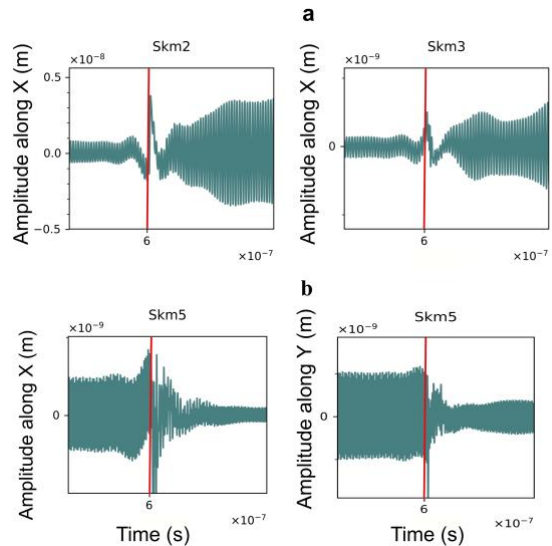


FIG. 4. Bursting and the reverse effect of the self-adaptive neuron. The figure plots the oscillatory output of the neuron in real-time, as it is reconfigured from Configuration II to I for driving frequencies of (a) 0.80 GHz and (b) 1.85 GHz. The neuron, in particular Sk2 and Sk3 for (a) and Sk5 for (b), demonstrates bursting properties as it transitions from oscillations with larger amplitudes to those with smaller amplitudes. The onset of reconfiguration is marked in red.

V. CONCLUSION

We design and simulate the functions of a novel artificial neuron which incorporates oscillatory dynamics and neuromodulation. The five coupled skyrmions in the bilayer of insulating thulium iron garnet (TmIG) and platinum (Pt) (TmIG/Pt) have resonant oscillatory modes that originate from skyrmion gyration, breathing, and the hybridizations of both. These modes have distinct resonant frequencies that shift upon the reconfiguration of the skyrmion lattice; therefore, the amplitude of the oscillatory output of the neuron also changes in response to the external oscillatory input of a certain frequency as the neuron is reconfigured. We demonstrate this neuromodulation effect by modeling the bursting as well as its reverse of T-SKONE, in which it exhibits a drastic increase or decrease of its skyrmion oscillation amplitudes as the skyrmion lattice is reconfigured in real time.

Although the functionality of T-SKONE is studied using five skyrmions in three lattice configurations, both the numbers and configurations of the skyrmions can be scaled up to increase the number of resonant modes and the range of neuromodulation. The dynamics of T-SKONE can empower a variety of neuromorphic applications. For example, bursting can be used for burst-coding, information multiplexing with different types of information encoded in spikes and bursts and for pacemakers in synchronous networks; moreover, the real-time tunability of neuronal dynamics along with its short-term memory can be utilized for reservoir computing-based online learning applications. By capturing advanced bio-plausible functionalities, T-SKONE has the potential of significantly advancing the development of generalized artificial intelligence.

VI. METHODS

Material parameters used for micromagnetic modeling of the TmIG/Pt system were taken from references [22] [27]: saturation magnetization $M_{\text{sat}} = 50 \times 10^3$ A/m, exchange stiffness $A_{\text{ex}} = 0.8 \times 10^{-12}$ J/m, interfacial Dzyaloshinskii-Moriya constant $D_{\text{ind}} = 50 \times 10^{-6}$ J/m², Gilbert damping constant $\alpha = 0.02$, perpendicular magnetic anisotropy (PMA) $K_{\text{u}} = 1.8 \times 10^3$ J/m³ and 2.0×10^3 J/m³ for the reduced anisotropy regions (pinning sites) and normal regions, respectively. The neuron consists of five nanotracks of width of 180 nm (along x , coordinates defined in Fig. 1). There were two high-anisotropy track regions of length 56 nm (along y) alternating between three low-anisotropy pinning wells of length 12 nm (along y). The neuron was padded along x and y with unpatterned magnetic material to enhance skyrmion stability and closed boundary conditions were employed. To calculate the FFT spectrum a sinc(x) driving field with a cut of frequency of 60 GHz and field strength of 4 mT was applied to all nanotracks for 1 ns. Subsequently, the neuron is allowed to relax, and its output was calculated. For simulations of the oscillatory dynamics, a sinusoidal driving field of 1 mT was applied to all nanotracks and the oscillatory output was calculated. The oscillations of the skyrmion cores along X and Y are taken to be the oscillatory output of the device.

VII. ACKNOWLEDGMENTS

The authors acknowledge funding from the National Science Foundation CAREER under award number 1940788, and computing resources from the Texas Advanced Computing Center (TACC) at the University of Texas at Austin (<http://www.tacc.utexas.edu>).

VIII. AUTHOR CONTRIBUTIONS

P. J. and C. C. share first authorship.

P. J. conceived the idea and designed the project. P. J. and C. C. carried out the calculations and J.A.I. led the project. P. J., C. C. and J. A. I. analyzed the data, discussed the results and wrote the manuscript.

IX. COMPETING INTERESTS STATEMENT

The authors declare no competing interests.

REFERENCES

- [1] I. Goodfellow, Y. Bengio and A. Courville, *Deep Learning*, The MIT Press, 2016.
- [2] Y. LeCun, Y. Bengio and G. Hinton, "Deep learning," *Nature*, vol. 521, p. 436–444, 2015.
- [3] P. A. Merolla, et al., "A million spiking-neuron integrated circuit with a scalable communication network and interface," *Science*, vol. 345, no. 6197, pp. 668–673, 2014.
- [4] E. Marder, "Dynamic Modulation of Neurons and Networks," in *Advances in Neural Information Processing Systems 6 (NIPS)*, 1993.
- [5] R. A. Silver, "Neuronal arithmetic," *Nature Reviews*, vol. 11, p. 474, 2010.
- [6] J. Torrejon, et al., "Neuromorphic computing with nanoscale spintronic oscillators," *Nature*, vol. 547, p. 428, 2017.
- [7] L. Gao, P.-Y. Chen and S. Yu, "NbOx based oscillation neuron for neuromorphic computing," *Appl. Phys. Lett.*, vol. 111, p. 103503, 2017.
- [8] R. F. Helfrich and R. T. Knight, "Oscillatory Dynamics of Prefrontal Cognitive Control," *Trends in Cognitive Sciences*, vol. 20, no. 12, p. 916, 2016.
- [9] C. Tallon-Baudry and O. Bertrand, "Oscillatory gamma activity in humans and its role in object representation," *Trends in Cognitive Sciences*, vol. 3, no. 4, p. 151, 1999.
- [10] W. Singer and C. M. Gray, "Visual feature integration and the temporal correlation hypothesis," *Annu. Rev. Neurosci.*, vol. 18, p. 555, 1995.
- [11] F. Nadim and D. Bucher, "Neuromodulation of Neurons and Synapses," *Curr Opin Neurobiol.*, vol. 0, p. 48–56, 2014.
- [12] M. E. Hasselmo and M. Sarter, "Modes and Models of Forebrain Cholinergic Neuromodulation of Cognition," *Neuropsychopharmacology Reviews*, vol. 36, p. 52–73, 2011.
- [13] A. Wutz, D. Melcher and J. Samaha, "Frequency modulation of neural oscillations according to visual task demands," *PNAS*, vol. 115, no. 6, p. 1346–1351, 2018.
- [14] G. Indiveri, "Modeling Selective Attention Using a Neuromorphic Analog VLSI Device," *Neural Computation*, vol. 12, p. 2857–2880, 2000.

- [15] M. Romera, et al., "Vowel recognition with four coupled spin-torque nano-oscillators," *Nature*, vol. 563, p. 230, 2018.
- [16] M. A. Azam, D. Bhattacharya, D. Querlioz and J. Atulasimha, "Resonate and fire neuron with fixed magnetic skyrmions," *Journal of Applied Physics*, vol. 124, no. 152122, 2018.
- [17] S. Li, et al., "Magnetic skyrmion-based artificial neuron device," *Nanotechnology*, vol. 28, no. 31LT01, 2017.
- [18] X. Chen, et al., "A compact skyrmionic leaky-integrate-fire spiking neuron device," *Nanoscale*, vol. 10, p. 6139, 2018.
- [19] M.-C. Chen, A. Sengupta and K. Roy, "Magnetic Skyrmion as a Spintronic Deep Learning Spiking Neuron Processor," *IEEE Transactions on Magnetics*, vol. 54, p. 1500207, 2018.
- [20] J. Wells, J. H. Lee, R. Mansell, R. P. Cowburn and O. Kazakova, "Controlled manipulation of domain walls in ultra-thin CoFeB nanodevices," *Journal of Magnetism and Magnetic Materials*, vol. 400, pp. 219-224, 2016.
- [21] K. Moon, B. Chun, W. Kim and C. Hwang, "Control of spin-wave refraction using arrays of skyrmions," *Physical Review Applied*, vol. 6, no. 6, p. 064027, 2016.
- [22] Q. Shao, Y. Liu, G. Yu, S. Kim, X. Che, C. Tang, Q. He, Y. Tserkovnyak, J. Shi and K. Wang, "Topological Hall effect at above room temperature in heterostructures composed of a magnetic insulator and a heavy metal," *Nature Electronics*, vol. 2, no. 5, pp. 182-186., 2019.
- [23] S. Vélez, J. Schaab, M. Wörnle, M. Müller, E. Gradauskaite, P. Welter, C. Gutgsell, C. Nistor, C. Degen, M. Trassin and M. Fiebig, "High-speed domain wall racetracks in a magnetic insulator," *Nature communications*, vol. 10, no. 1, pp. 1-8, 2019.
- [24] C. Avci, E. Rosenberg, L. Caretta, F. Büttner, M. Mann, C. Marcus, D. Bono, C. Ross and G. Beach, "Interface-driven chiral magnetism and current-driven domain walls in insulating magnetic garnets," *Nature nanotechnology*, vol. 14, no. 6, pp. 561-5, 2019.
- [25] A. Vansteenkiste, J. Leliaert, M. Dvornik, M. Helsen, F. Garcia-Sanchez and B. Van Waeyenberge, "The design and verification of MuMax3," *AIP advances*, vol. 4, no. 10, p. 107133, 2014.
- [26] J. Kim, J. Yang, Y. Cho, B. Kim and S. Kim, "Coupled gyration modes in one-dimensional skyrmion arrays in thin-film nanostrips as new type of information carrier," *Scientific reports*, vol. 7, p. 45185, 2017.
- [27] O. Ciubotariu, A. Semisalova, K. Lenz and M. Albrecht, "Strain-induced perpendicular magnetic anisotropy and Gilbert damping of Tm₃Fe₅O₁₂ thin films," *Scientific reports*, vol. 9, no. 1, pp. 1-8, 2019.